iScience

CellPress
OPEN ACCESS

Article

circAGTPBP1 promotes the progression of papillary thyroid cancer through the notch pathway via the miR-34a-5p/notch1 axis

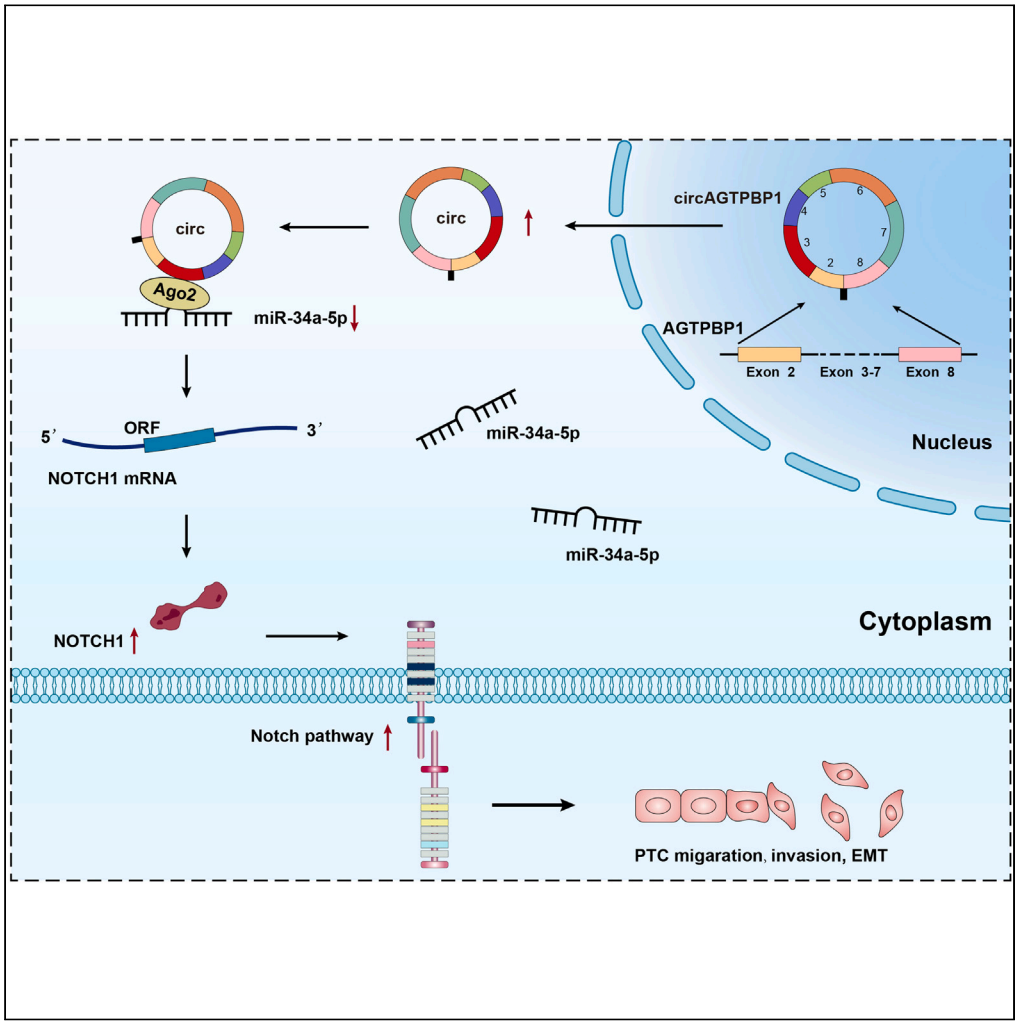

Lei Dai, Weidong Zhang, Yinchun Wang, Kejie Yu, Qi Le, Xianjiang Wu

wuxianjiangtg@163.com

Highlights

circAGTPBP1 promotes the migration, invasion, and metastasis of PTC

circAGTPBP1 promotes PTC progression via the miR-34a-5p/Notch1 axis

circAGTPBP1 knockdown inhibited tumor growth *in vivo*

Dai et al., iScience *26*, 107564
September 15, 2023
https://doi.org/10.1016/j.isci.2023.107564

iScience

CellPress
OPEN ACCESS

Article

circAGTPBP1 promotes the progression of papillary thyroid cancer through the notch pathway via the miR-34a-5p/notch1 axis

Lei Dai,[1] Weidong Zhang,[1] Yinchun Wang,[1] Kejie Yu,[1] Qi Le,[1] and Xianjiang Wu[1,2,*]

SUMMARY

The dysregulation of circular RNAs (circRNAs) has been implicated in the development and progression of papillary thyroid cancer (PTC). In this study, we analyzed the dysregulated circRNA profile using PTC tissues and matched adjacent normal tissues by RNA-seq. We conducted *in vitro* and *in vivo* experiments to investigate the biological functions of circAGTPBP1 in PTC progression. We found that circAGTPBP1 was upregulated in PTC tissues and cell lines, and its expression was positively correlated with tumor size, lymph node metastasis, and clinical stage. Using RNA-seq and bioinformatic analysis, we identified miR-34a-5p and NOTCH1 as downstream targets of circAGTPBP1. Functionally, circAGTPBP1 knockdown significantly inhibited the migration, invasion, and metastasis of PTC cell lines *in vitro*, while the miR-34a-5p inhibitor reversed these effects. Additionally, circAGTPBP1 knockdown inhibited tumor growth *in vivo*. Our findings suggest that circAGTPBP1 may act as a tumor promoter and could be a potential therapeutic target for PTC.

INTRODUCTION

Thyroid cancer has become the most common endocrine malignancy worldwide, with a rapidly increasing incidence.[1] Cancer statistics in China show that approximately 67,900 females and 22,000 males are diagnosed with thyroid cancer every year.[2] Among all thyroid cancers, papillary thyroid cancer (PTC) is the most prevalent and threatening subtype.[3] Although satisfactory treatment outcomes are generally achieved, advanced-stage patients often face poor outcomes due to uncontrollable invasion and metastasis of PTC.[4] Therefore, exploring the molecular mechanisms of PTC progression and metastasis and identifying potential therapeutic targets are crucial.

Circular RNAs (circRNAs) are a new class of endogenous noncoding RNAs that may regulate gene expression in mammals and play critical roles in various biological processes.[5,6] CircRNAs, derived from introns, exons, or intergenic regions, have a complete covalently closed loop structure and are highly conserved in mammalian cells due to their resistance to RNase R.[7,8] Emerging evidence suggests that dysregulated circRNAs play important roles in the progression and metastasis of various tumors, including PTC.[9–11] A previous study demonstrated that the upregulation of circRNA_102171 promotes the progression of PTC by activating the Wnt/β-catenin pathway by interacting with CTNNBIP1 to block its interaction with the β-catenin/TCF3/TCF4/LEF1 complex.[12] Another study indicated that hsa_circ_0058124, acting as an oncogenic driver, promotes the tumorigenicity, cell proliferation, cell invasion, and metastasis of PTC by regulating the NOTCH3/GATAD2A signaling pathway via the miRNA-218-5p/NUMB axis.[13] Similarly, Zhang et al.[14] emphasized that circTIAM1 plays a crucial role in promoting the progression of papillary thyroid carcinoma by targeting microRNA-646 and heterogeneous ribonucleoprotein A1.

In this study, we focused on circAGTPBP1, which was significantly upregulated in PTC tissues and cell lines compared to normal controls. Our *in vitro* and *in vivo* experiments demonstrated that circAGTPBP1 could promote PTC progression by regulating the Notch pathway through sponging miR-34a-5p and releasing NOTCH1. We highlight the pathogenetic role of the circAGTPBP1/miR-34a-5p/NOTCH1 axis in PTC progression, and this study provides a potential therapeutic insight into PTC.

RESULTS

Identification, expression, and characterization of circAGTPBP1

To investigate the involvement of circRNAs in the progression of PTC, we conducted RNA-seq analyses on total RNA extracted from 4 paired PTC and adjacent normal thyroid tissues (for clinical information, see Table 1). In total, we identified 17,642 distinct circRNAs in our circRNA profiling database, 17,203 of which have been previously reported in the circBase database (Figure 1A). Figure 1B shows the length distribution of the detected circRNAs, with most of the circRNAs having a length of less than 500 nucleotides or more than 2000 nucleotides. The genomic origin of the circRNAs is presented in Figures 1C and 1D shows the volcano plot, and Figure 1E shows

[1]Department of Thyroid Surgery, Ningbo No.2 Hospital,No. 41 Xibei Street, Ningbo City 315000, Zhejiang Province, China
[2]Lead contact
*Correspondence: wuxianjiangtg@163.com
https://doi.org/10.1016/j.isci.2023.107564

Table 1. Patient demographics associated with circAGTPBP1 expression

	circAGTPBP1 expression		
Characteristics	Low	High	p value
Number	25	25	–
Gender	–	–	0.758
Male	8	7	–
Female	17	18	–
Age (years)	–	–	0.571
≥45	11	13	–
<45	14	12	–
Tumor size (cm)	–	–	0.024
≥1	8	16	–
<1	17	9	–
TNM stage	–	–	0.004
I/II	20	10	–
III/IV	5	15	–
Lymph node metastasis	–	–	0.007
Positive	4	13	–
Negative	21	12	–

Median circAGTPBP1 value was used as the cutoff.

the cluster heatmap (presenting the top 50 dysregulated circRNAs) of significantly dysregulated circRNAs (235 upregulated and 176 downregulated) in PTC tissues compared to matched adjacent tissues ($|\log_2$ fold change (FC)| > 2 and p value < 0.05). Among the 411 dysregulated circRNAs, we focused on hsa_circ_0087391 (circAGTPBP1), which was the most upregulated circRNA in our RNA-seq data. To validate the dysregulated expression of circAGTPBP1 in PTC, we performed qRT-PCR on 50 paired PTC and adjacent normal thyroid tissue samples. The results confirmed that the expression level of circAGTPBP1 was significantly increased in PTC tissues compared to adjacent tissues (Figure 1F), consistent with our RNA-seq data. However, there was no significant difference in AGTPBP1 mRNA levels between adjacent and PTC tissues (Figure 1G). Our results indicated that circAGTPBP1 expression was closely associated with tumor size (Figure 1H), lymph node metastasis (Figure 1I), and TNM stage (Figure 1J), suggesting a strong correlation between circAGTPBP1 and PTC progression.

circAGTPBP1 originates from AGTPBP1, which is located at chromosome 9 (chr9: 88284399–88327481) (Figure 2A). It is formed by the back-splicing of exon 2 and exon 8, resulting in a full length of 695 nt (Figure 2B). Sanger sequencing confirmed the back-splicing site (Figure 2C), and the predicted minimum free energy (MFE) and centroid secondary structures of circAGTPBP1 were analyzed using RNAfold WebServer (Figure 2D).[15] To evaluate the expression levels of circAGTPBP1, we assessed its expression in several PTC cell lines, including B-CPAP, TPC-1, K1, IHH-4, and KTC-1 cell lines, relative to the Nthy-ori 3-1 cell line (Figure 2E). Among the PTC cell lines, B-CPAP and TPC-1 showed the lowest and highest expression of circAGTPBP1, respectively. We consider the heterogeneity across the cell lines and some other factors (e.g., measurement error, etc.) might be possible explanations for the differences. Thus, we chose these two cell lines to further investigate the biological functions and mechanisms of circAGTPBP1. We performed RNase R experiments to evaluate the stability of circAGTPBP1, and the results indicated that circAGTPBP1 was resistant to RNase R digestion in TPC-1 and B-CPAP cell lines (Figure 2F). Divergent and convergent primers were designed to amplify circAGTPBP1 and GAPDH mRNAs. Agarose gel electrophoresis and PCR assays indicated that circAGTPBP1 was only amplified by divergent primers in cDNA (Figure 2G). Next, we performed FISH analysis to investigate the intracellular localization of circAGTPBP1 (Figure 2H). As shown in Figure 2I, qRT-PCR analysis indicated that circAGTPBP1 was mainly expressed in the cytoplasm, indicating that it may serve as a "ceRNA" molecule. Overall, circAGTPBP1 was confirmed as a PTC-associated circRNA with good stability, which is worthy of further functional and mechanistic studies.

Biological functions of circAGTPBP1 in PTC

To explore the biological functions of circAGTPBP1 in PTC, we designed three siRNAs to knock down circAGTPBP1 expression. The qRT-PCR results showed that si-circAGTPBP1-1 exhibited the most significant inhibitory effect on circAGTPBP1 expression in both TPC-1 and B-CPAP cell lines, so it was selected for further experiments (Figure 3A). CCK-8 assays demonstrated that downregulation of circAGTPBP1 led to a significant decrease in the viability and proliferation of TPC-1 and B-CPAP cell lines (Figure 3B). Colony formation and EdU assays further confirmed that knockdown of circAGTPBP1 significantly attenuated colony formation and decreased the percentages of EdU-positive TPC-1 and B-CPAP cells (Figures 3C and 3D). We also evaluated the effect of circAGTPBP1 on the migration and invasion capabilities of

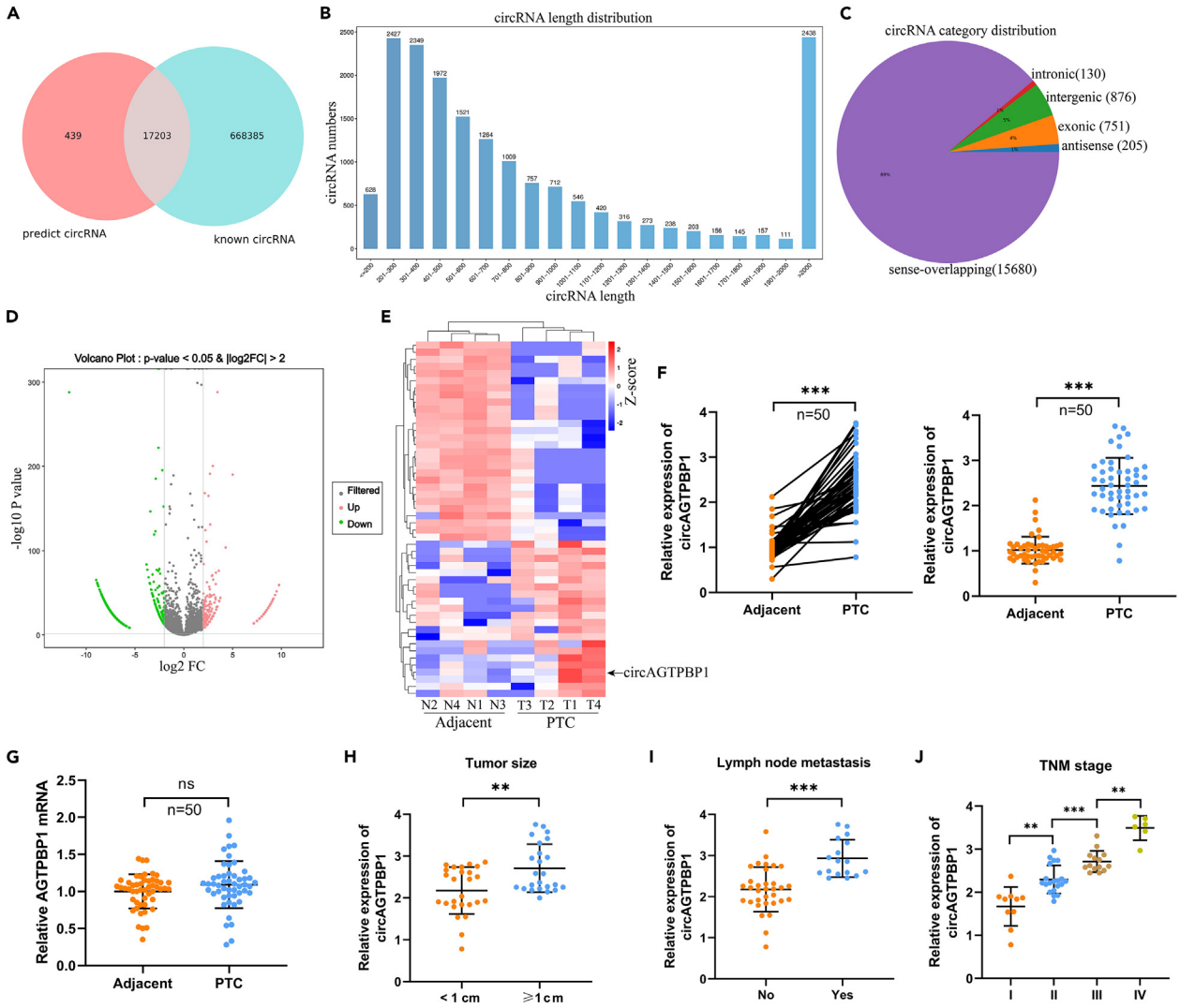

Figure 1. Identification of circAGTPBP1 in PTC

(A) Overlap of circRNAs in RNA-seq (left) and circBase (right).

(B) Length distribution of circRNAs.

(C) Composition of the detected circRNAs in terms of genomic origin.

(D) Volcano plots showing the circRNA expression profile in PTC and adjacent normal thyroid tissues (|log2 FC| > 2 and $p < 0.05$).

(E) Heatmap showing the top 50 dysregulated circRNAs (|log2 FC| > 2 and $p < 0.05$). Relative circAGTPBP1.

(F–J) and AGTPBP1 mRNA (G) expression in PTC (n = 50) and adjacent normal thyroid tissues (n = 50) by qRT-PCR analysis. Relationship between circAGTPBP1 expression level and tumor size (H), lymph node metastasis (I), and clinical TNM stage (J) (n = 50). Each experiment was repeated three times with triplicates. PTC, papillary thyroid cancer; FC, fold change; qRT-PCR, quantitative real-time polymerase chain reaction. Data are shown as the mean ± SD, ns indicates no significance. **$p < 0.01$, ***$p < 0.001$. Paired t test for (F) and (G), unpaired t test for (H) and (I), and one-way analysis of variance (ANOVA) test for (J).

TPC-1 and B-CPAP cells using wound healing and Transwell assays. The results showed that circAGTPBP1 knockdown significantly suppressed the migration and invasion of TPC-1 and B-CPAP cells (Figures 3E and 3F). Additionally, we assessed the effect of circAGTPBP1 on the epithelial-mesenchymal transition (EMT) process by examining EMT markers (E-cadherin and N-cadherin) and morphological changes. The findings suggested that knockdown of circAGTPBP1 inhibited the EMT properties of TPC cells (Figures 3G and 3H).

Identification of miR-34a-5p as a target miRNA of circAGTPBP1

To investigate the potential target miRNAs of circAGTPBP1 based on the ceRNA theory, we utilized online prediction tools and identified six candidate miRNAs through the overlap of the starBase and circBank databases (Figure 4A). Among the six candidate miRNAs, hsa-miR-145-5p, and hsa-miR-34a-5p were further validated using circMIR software (http://www.bioinf.com.cn), which is based on miRanda and RNAhybrid

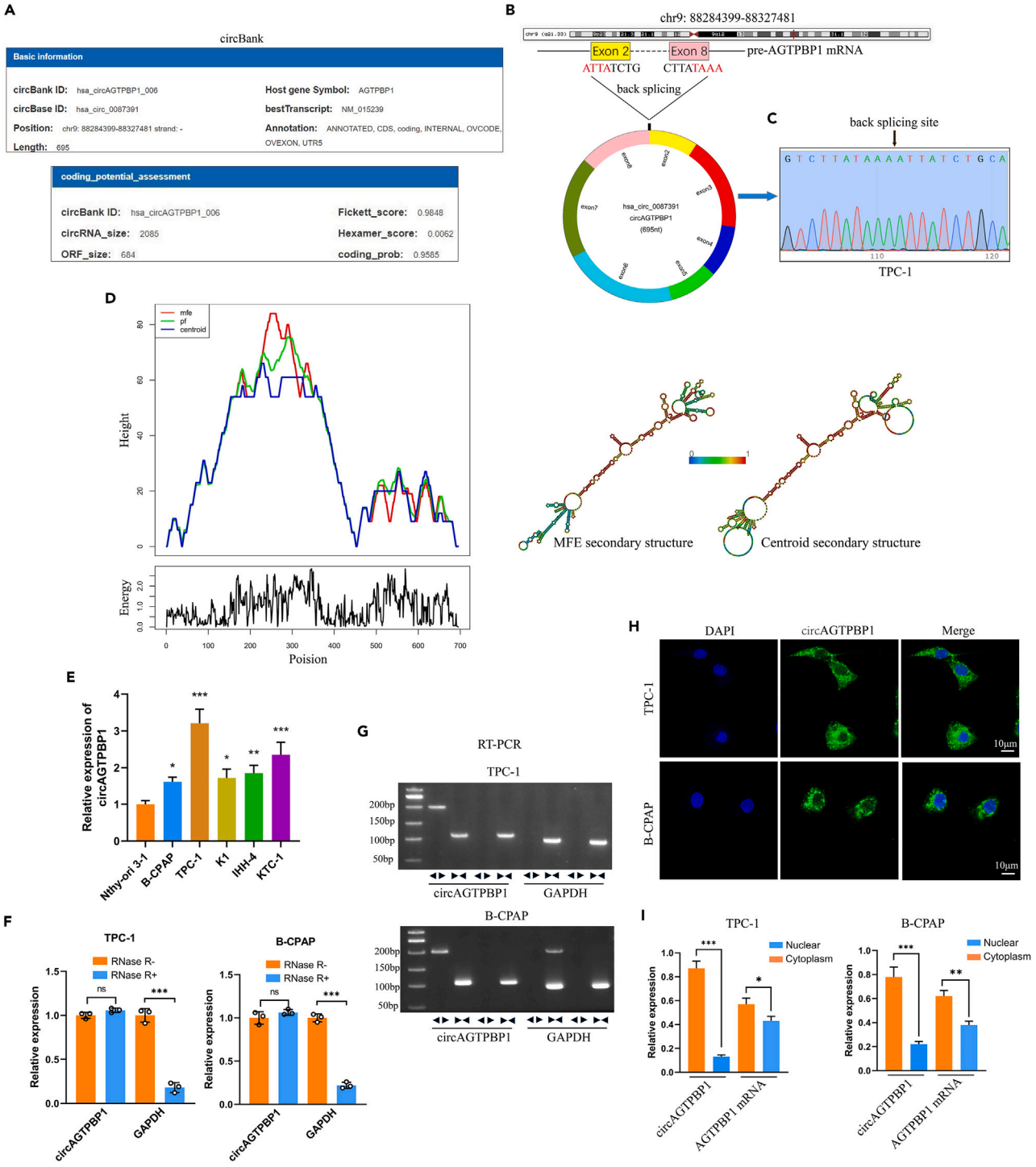

Figure 2. Characteristics of circAGTPBP1 in PTC

(A) Basic information and coding potential assessment by circBank.

(B) The circular structure of circAGTPBP1 back-spliced by exon 2 and exon 8.

(C) The splicing of circAGTPBP1 by Sanger sequencing in TPC-1 cell lines.

(D) The predicted secondary structures of circAGTPBP1.

(E) Relative circAGTPBP1 expression in different cell lines.

(F) RNase R treatment experiments followed by qRT-PCR analyses.

Figure 2. *Continued*

(G) The expression of circAGTPBP1 in TPC-1 and B-CPAP cell lines according to RT-PCR. circAGTPBP1 was amplified by divergent primers in cDNA but not gDNA.

(H) The localization of circAGTPBP1 in TPC-1 and B-CPAP cell lines according to FISH analysis. Scale bar: 10 μm.

(I) The expression of circAGTPBP1 in the nucleus and cytoplasm of TPC-1 and B-CPAP cell lines according to qRT-PCR. Each experiment was repeated three times with triplicates. PTC, papillary thyroid cancer; FISH, fluorescence *in situ* hybridization; DAPI, 4,6-Diamidine-2-phenylindole; qRT-PCR, quantitative real-time polymerase chain reaction; MFE, minimum free energy. Data are shown as the mean ± SD, ns indicates no significance. **p < 0.01, ***p < 0.001. Unpaired t test for (F) and (I), and one-way analysis of variance (ANOVA) test for (E).

algorithms. Subsequently, qRT-PCR analysis was performed to evaluate the expression of miR-145-5p and miR-34a-5p in 50 paired PTC and adjacent normal thyroid tissues. The results revealed that there was no significant difference in the expression levels of miR-145-5p between PTC and adjacent normal tissues (Figure 4B), while the relative expression levels of miR-34a-5p were significantly higher in adjacent normal tissues than in PTC tissues (Figure 4C). Therefore, miR-34a-5p was selected as a potential target miRNA of circAGTPBP1 for further investigation. Moreover, qRT-PCR analysis demonstrated a significant correlation between miR-34a-5p expression and lymph node metastasis (Figure 4D) as well as TNM stage (Figure 4E). Additionally, FISH analyses revealed that circAGTPBP1 and miR-34a-5p were mainly expressed in the cytoplasm of PTC tissues and adjacent thyroid tissues (Figure 4F). A negative correlation between the relative expression levels of circAGTPBP1 and miR-34a-5p was identified by qRT-PCR analysis (Figure 4G).

Moreover, using circBank, starBase database, and oeCloud based on the miRanda algorithm (Figure 5A), we predicted the binding site between circAGTPBP1 and miR-34a-5p. Colocalization of circAGTPBP1 and miR-34a-5p was also observed in TPC-1 and B-CPAP cells through the FISH assay (Figure 5B). Dual-luciferase reporter assays showed that the luciferase reporter vector carrying the circAGTPBP1 3′UTR-WT sequence had decreased activity in the miR-34a-5p mimic group vs. control group but increased activity in the miR-34a-5p inhibitor group (Figure 5C), and no significant difference was observed in the activity of the reporter for mutated circAGTPBP1. To further confirm these findings, we overexpressed or knocked down circAGTPBP1 and analyzed the effects on the expression of circAGTPBP1 and miR-34a-5p. Our qRT-PCR results demonstrated that circAGTPBP1 overexpression suppressed miR-34a-5p, while circAGTPBP1 knockdown significantly increased miR-34a-5p expression in TPC-1 cells (Figure 5D). Additionally, Ago2 RIP experiments followed by qRT-PCR analyses revealed that both circAGTPBP1 and miR-34a-5p were highly enriched in TPC-1 cells transfected with the miR-34a-5p mimic compared to the control group (Figure 5E). Furthermore, a biotinylated RNA pull-down assay showed that both circAGTPBP1 and miR-34a-5p were highly enriched in the circAGTPBP1 probe group, and circAGTPBP1 was also highly enriched in the biotin-labeled miR-34a-5p group (Figure 5F). Taken together, these results strongly support the conclusion that miR-34a-5p is a target miRNA of circAGTPBP1.

Identification of NOTCH1 as a target gene of miR-34a-5p

MiR-34a-5p targets were identified by overlapping candidates identified by mRNA sequencing data and bioinformatic analyses. A volcano plot (Figure 6A) and a heatmap (Figure 6B) based on RNA sequencing data were generated to compare expression in PTC and adjacent normal thyroid tissues. The analysis revealed that 137 mRNAs were dysregulated (59 upregulated and 78 downregulated) in PTC tissues compared to adjacent tissues (|log2-fold change (FC)| > 2 and p value < 0.05). Different algorithms were used to assess the upregulated mRNAs, NOTCH1 was identified as a candidate target gene of miR-34a-5p (Figure 6C). Furthermore, qRT-PCR analysis confirmed that NOTCH1 expression was significantly upregulated in PTC tissues compared to adjacent tissues (Figure 6D). Additionally, relative NOTCH1 expression level was found to be correlated with lymph node metastasis (Figure 6E) and TNM stage (Figure 6F). The predicted binding site between miR-34a-5p and NOTCH1 was based on the starBase database (Figure 6G). Dual-luciferase reporter analysis revealed that the luciferase reporter vector carrying the NOTCH1 3′UTR-WT sequence showed significantly decreased activity in TPC-1 and B-CPAP cells transfected with the miR-34a-5p mimic vs. control cells and increased activity in cells transfected with the miR-34a-5p inhibitor (Figure 6H). However, no significant difference was observed in the activity of the reporter for mutated NOTCH1 (Figure 6H). Moreover, in both TPC-1 and B-CPAP cells, the miR-34a-5p mimic significantly decreased NOTCH1 expression, while the miR-34a-5p inhibitor increased NOTCH1 expression (Figure 6I). Taken together, these results strongly suggest that NOTCH1 is a target gene of miR-34a-5p.

"ceRNA" network verification and rescue experiments

To confirm the circAGTPBP1/miR-34a-5p/NOTCH1 network, we conducted experiments to examine the impact of circAGTPBP1 and miR-34a-5p on NOTCH1 expression. Our findings demonstrated that overexpression of circAGTPBP1 (oe-circAGTPBP1) significantly increased the expression of NOTCH1, and this effect was reversed by the miR-34a-5p mimic. On the other hand, knockdown of circAGTPBP1 (si-circAGTPBP1) reduced NOTCH1 expression, and this effect was reversed by the miR-34a-5p inhibitor in both TPC-1 and B-CPAP cells (Figure 7A). Furthermore, colony formation assays revealed that the decreased in the number of colonies caused by si-circAGTPBP1 was reversed by the miR-34a-5p inhibitor, while the increased in number of colonies induced by oe-circAGTPBP1 was reversed by the miR-34a-5p mimic (Figure 7B). In addition, circAGTPBP1 knockdown inhibited cell migration and invasion, and the effects were reversed by the miR-34a-5p inhibitor in TPC-1 cells. Similarly, the miR-34a-5p mimic reversed the stimulatory effect of circAGTPBP1 overexpression on migration and invasion in B-CPAP cells (Figure 7C). Moreover, si-circAGTPBP1 transfection increased E-cadherin protein expression and decreased N-cadherin and vimentin protein expression in TPC-1 cells. Conversely, oe-circAGTPBP1 transfection decreased E-cadherin protein levels and increased N-cadherin and vimentin protein levels in B-CPAP cells. The effects of oe-/si-circAGTPBP1 on EMT were reversed by the

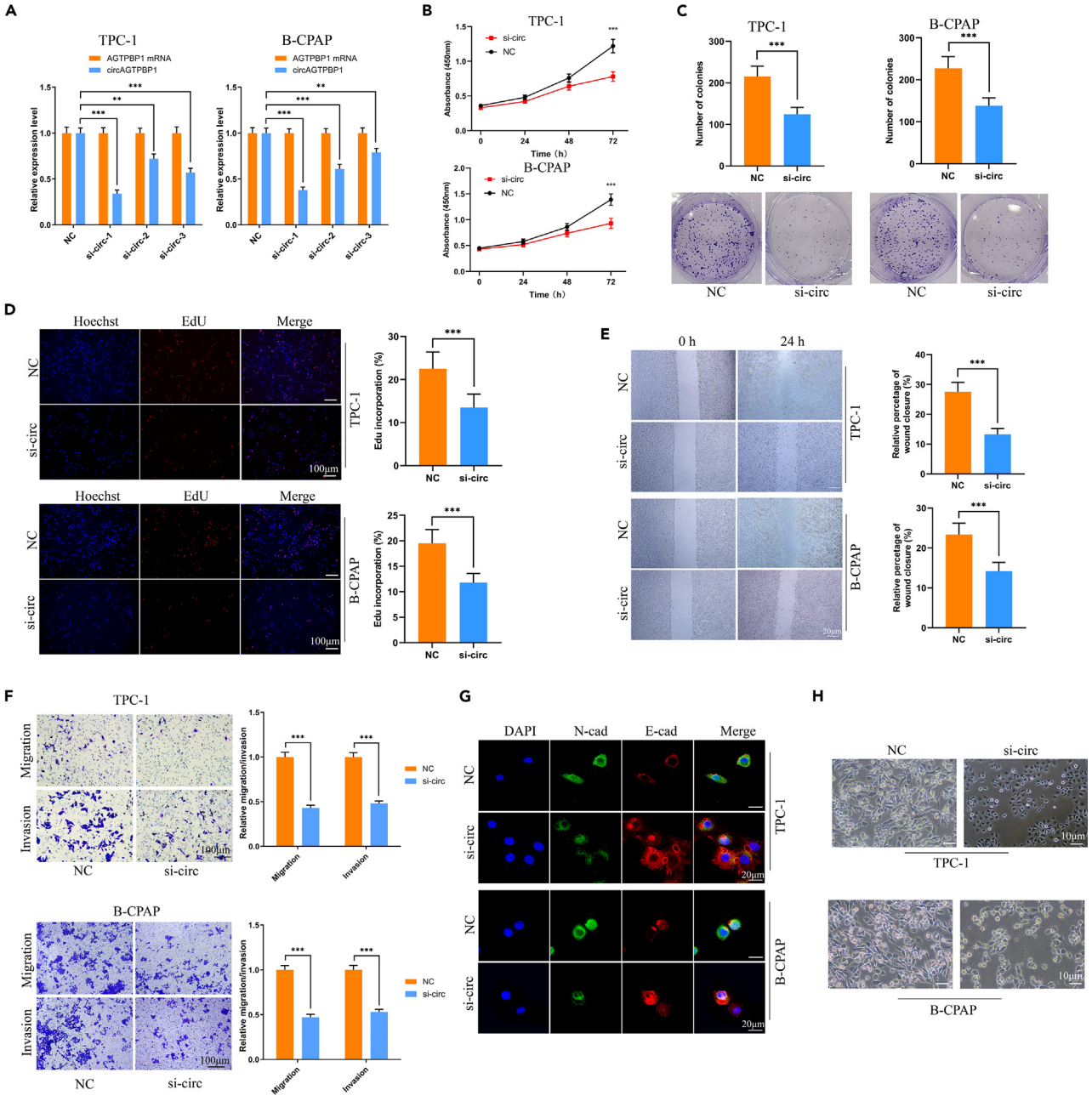

Figure 3. Biological functions of circAGTPBP1 in PTC

(A–F) qRT-PCR analysis of circAGTPBP1 and AGTPBP1 mRNA in TPC-1 and B-CPAP cell lines treated with three designed siRNAs. Proliferation ability of TPC-1 and B-CPAP cells transfected with si-circAGTPBP1 or NC as determined by CCK-8 (B), colony formation (C) and EdU assays (D). Scale bar: 100 μm. The migratory and invasive capabilities of TPC-1 and B-CPAP cells transfected with si-circAGTPBP1 or NC as assessed by wound healing (E, Scale bar: 20 μm) and Transwell assays (F).

(G) Immunofluorescence of E-cad and N-cad in TPC-1 and B-CPAP cells transfected with si-circAGTPBP1 or NC. Scale bar: 20 μm.

(H) Morphological changes in TPC-1 cells transfected with si-circAGTPBP1 or NC. Scale bar: 10 μm. Each experiment was repeated three times with triplicates. PTC, papillary thyroid cancer; DAPI, 4,6-Diamidine-2-phenylindole; qRT-PCR, quantitative real-time polymerase chain reaction; NC, normal control; CCK-8, cell counting kit-8. Data are shown as the mean ± SD, **p < 0.01, ***p < 0.001. Unpaired t test for (B), (C), (D), (E), and (F); one-way analysis of variance (ANOVA) test for (A).

miR-34a-5p mimic/inhibitor treatment (Figures 7D and 7E). NOTCH1 is a key component of the NOTCH signaling pathway, which plays a significant role in the progression of various tumors. Therefore, we further investigated the effects of circAGTPBP1 on the NOTCH pathway. The results indicated that knockdown of circAGTPBP1 significantly decreased the protein levels of NOTCH1, Hes1, and Jagged1, while

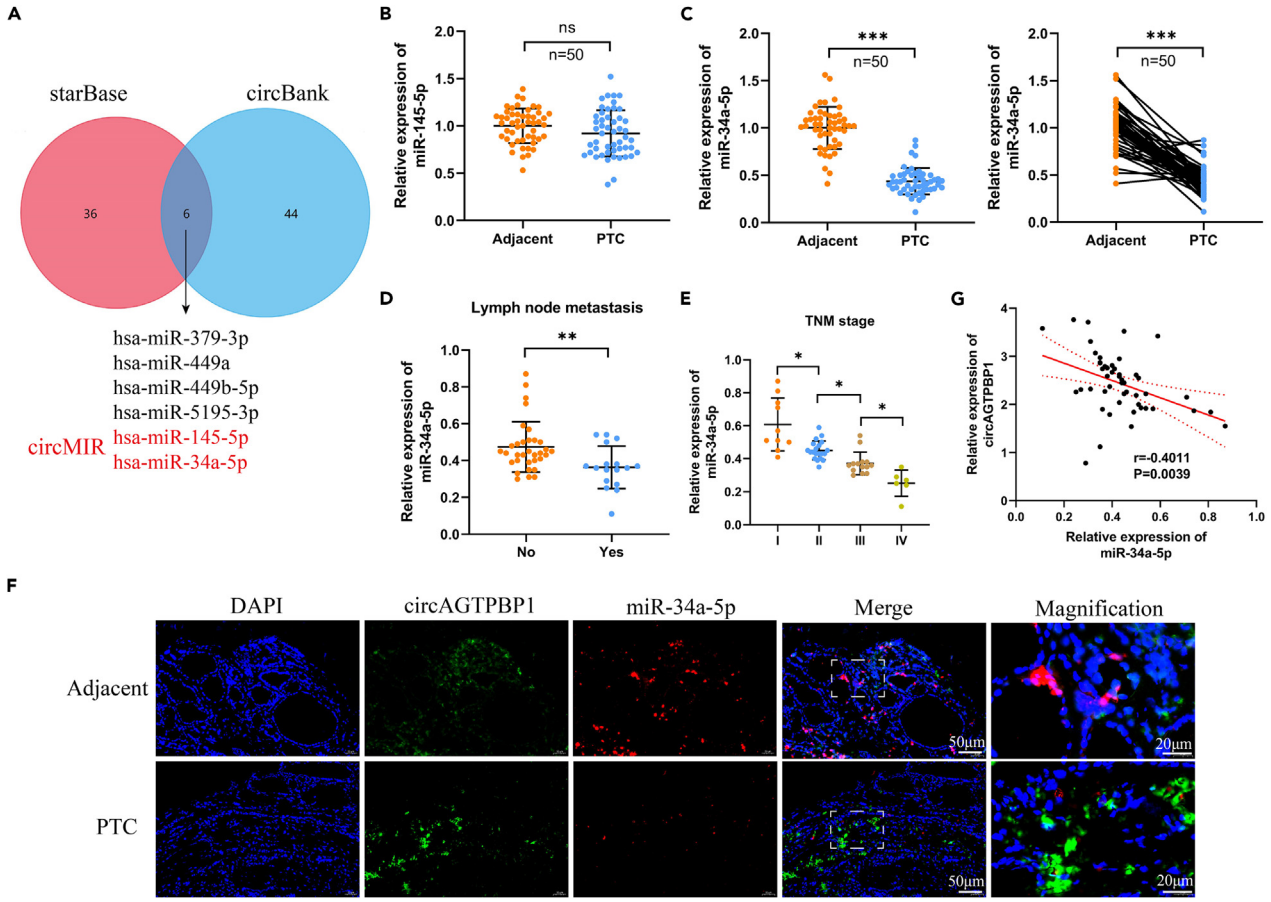

Figure 4. miR-34a-5p was identified as a target miRNA of circAGTPBP1

(A–E) Overlapping target miRNAs of circAGTPBP1 predicted by starBase and circBank. Relative miR-145-5p (B) and miR-34a-5p (C) expression in PTC (n = 50) and adjacent normal thyroid tissues (n = 50) by qRT-PCR analysis. Relationship between miR-34a-5p expression level and lymph node metastasis (D) and clinical TNM stage (E) (n = 50).

(F) FISH analyses of circAGTPBP1 and miR-34a-5p in PTC and adjacent normal thyroid tissues. Scale bar: 20 or 50 μm.

(G) Correlation between circAGTPBP1 and miR-34a-5p expression in PTC patients (n = 50).

PTC, papillary thyroid cancer; FISH, fluorescence *in situ* hybridization; DAPI, 4,6-Diamidine-2-phenylindole; qRT−PCR, quantitative real-time polymerase chain reaction. Data are shown as the mean ± SD, **p < 0.01, ***p < 0.001. Paired t test for (B) and (C), unpaired t test for (D), and one-way analysis of variance (ANOVA) test for (E).

circAGTPBP1 overexpression increased the levels of these proteins (Figures 7F and 7G). The effects of oe-/si-circAGTPBP1 on the NOTCH pathway were reversed by the miR-34a-5p mimic/inhibitor (Figures 7F and 7G).

circAGTPBP1 knockdown inhibited PTC growth *in vivo*

We conducted *in vivo* experiments to investigate the effect of circAGTPBP1 knockdown on PTC growth. Nude mice were injected with TPC-1 cells transfected with either control or sh-circAGTPBP1 (n = 6 per group). The results showed that the tumor volume (Figures 8A and 8B) and weight (Figure 8C) were significantly reduced in the sh-circAGTPBP1 group compared to the NC group. Additionally, the mRNA expression levels of circAGTPBP1 (Figure 8D) and NOTCH1 (Figure 8E) were significantly decreased in tumor tissues of the sh-circAGTPBP1 group, while miR-34a-5p expression (Figure 8F) was increased compared to that in the NC group. The corresponding excised lungs and histopathological analysis indicated that the number of nodules in the lung of sh-circAGTPBP1 group significantly decreased in comparison with that in the NC group (Figures 8G and 8H). These findings suggest that circAGTPBP1 may promote PTC progression and EMT by modulating the NOTCH signaling pathway through the miR-34a-5p/NOTCH1 axis (Figure 8I).

DISCUSSION

PTC is currently the most common endocrine malignancy with an increasing incidence worldwide.[16] Although most patients exhibit a satisfactory curative effect, some patients show quick progression, lymph node metastasis and distant metastasis, which results in poor

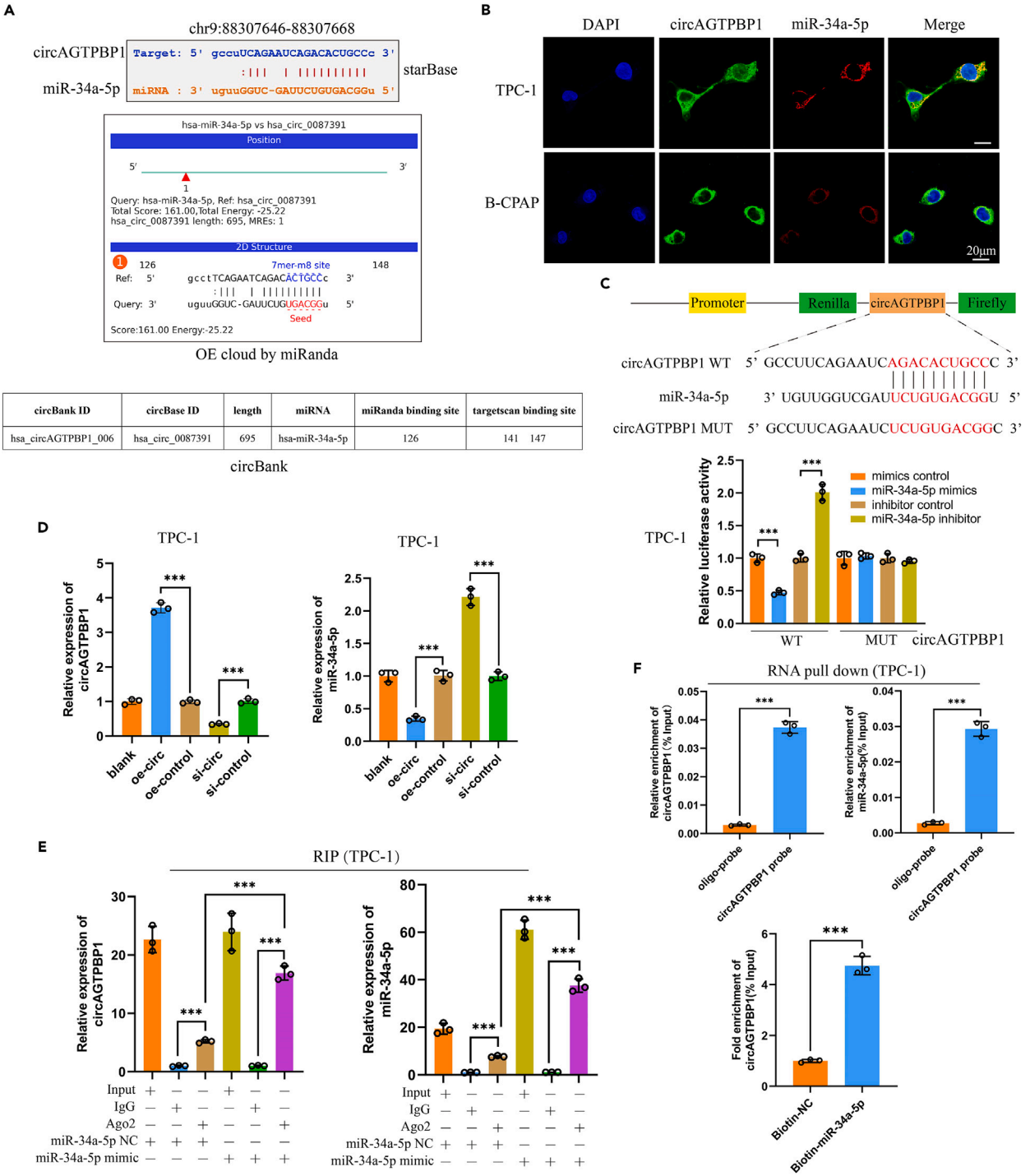

circBank ID	circBase ID	length	miRNA	miRanda binding site	targetscan binding site
hsa_circAGTPBP1_006	hsa_circ_0087391	695	hsa-miR-34a-5p	126	141 147

Figure 5. The interaction between miR-34a-5p and circAGTPBP1

(A) The predicted binding site between circAGTPBP1 and miR-34a-5p according to starBase, oeCloud, and circBank.

(B) Cellular locations of circAGTPBP1 and miR-34a-5p in TPC-1 and B-CPAP cell lines according to FISH analysis. Scale bar: 20 μm.

(C) Dual-luciferase reporter analysis in TPC-1 and B-CPAP cells transfected with circAGTPBP1-WT, circAGTPBP1-MUT, or miR-34a-5p mimic, inhibitor, or control.

(D) Relative circAGTPBP1 and miR-34a-5p expression in TPC-1 cells transfected with oe-circAGTPBP1, si-circAGTPBP1, or control.

(E) Ago2 RIP assay in TPC-1 cells transfected with the miR-34a-5p mimic and NC, followed by qRT-PCR to detect circAGTPBP1 and miR-34a-5p.

(F) RNA pull-down assay in TPC-1 cells, followed by qRT-PCR to detect the relative enrichment of circAGTPBP1 and miR-34a-5p. Each experiment was repeated three times with triplicates. PTC, papillary thyroid cancer; DAPI, 4,6-Diamidine-2-phenylindole; qRT−PCR, quantitative real-time polymerase chain reaction; NC, normal control; WT, wild type; MUT, mutant. Data are shown as the mean ± SD, **p < 0.01, ***p < 0.001 by one-way analysis of variance (ANOVA).

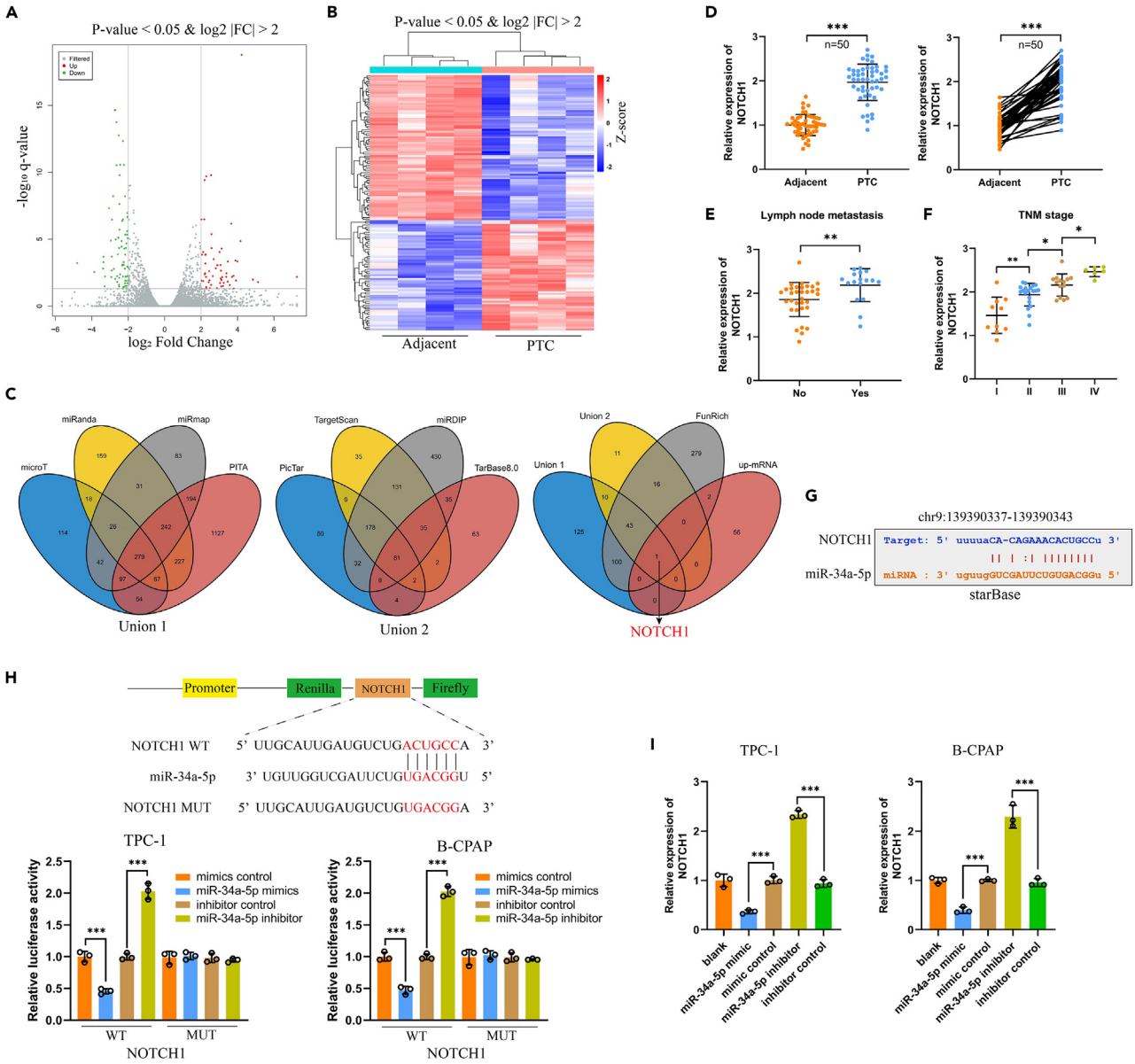

Figure 6. Identification of NOTCH1 as a target gene of miR-34a-5p

(A and B) Volcano plots (A) and heatmap (B) showing the dysregulated mRNA expression profile in PTC and adjacent normal thyroid tissues (|log2 FC| > 2 and p < 0.05).

(C) Overlap of predicted target genes of miR-34a-5p by different algorithms and upregulated mRNAs.

(D–F) Relative NOTCH1 expression in PTC and adjacent normal thyroid tissues by qRT-PCR (n = 50). Relationship between relative NOTCH1 expression and lymph node metastasis (E) and clinical TNM stage (F) (n = 50).

(G) The predicted binding site between miR-34a-5p and NOTCH1 according to starBase.

(H) Dual-luciferase reporter analysis in TPC-1 and B-CPAP cells transfected with NOTCH1-WT, NOTCH1-MUT, or miR-34a-5p mimic, inhibitor, or control.

(I) Relative NOTCH1 expression in TPC-1 and B-CPAP cells transfected with miR-34a-5p mimic, inhibitor, or control. Each experiment was repeated three times with triplicates. PTC, papillary thyroid cancer; qRT-PCR, quantitative real-time polymerase chain reaction; NC, normal control; FC, fold change; WT, wild type; MUT, mutant. Data are shown as the mean ± SD, **p < 0.01, ***p < 0.001. Paired t test for (D), unpaired t test for (E), and one-way analysis of variance (ANOVA) test for (F), (H), and (I).

prognosis.[17,18] Thus, it is of great importance to elucidate the underlying mechanisms and investigate potential therapeutic targets for PTC. Accumulating evidence concerning the biological functions of circRNAs has offered a perspective on the pathogenesis of various diseases, including cancer[19] and autoimmune disease.[20] Previous studies have indicated that some circRNAs can function as tumor suppressors or

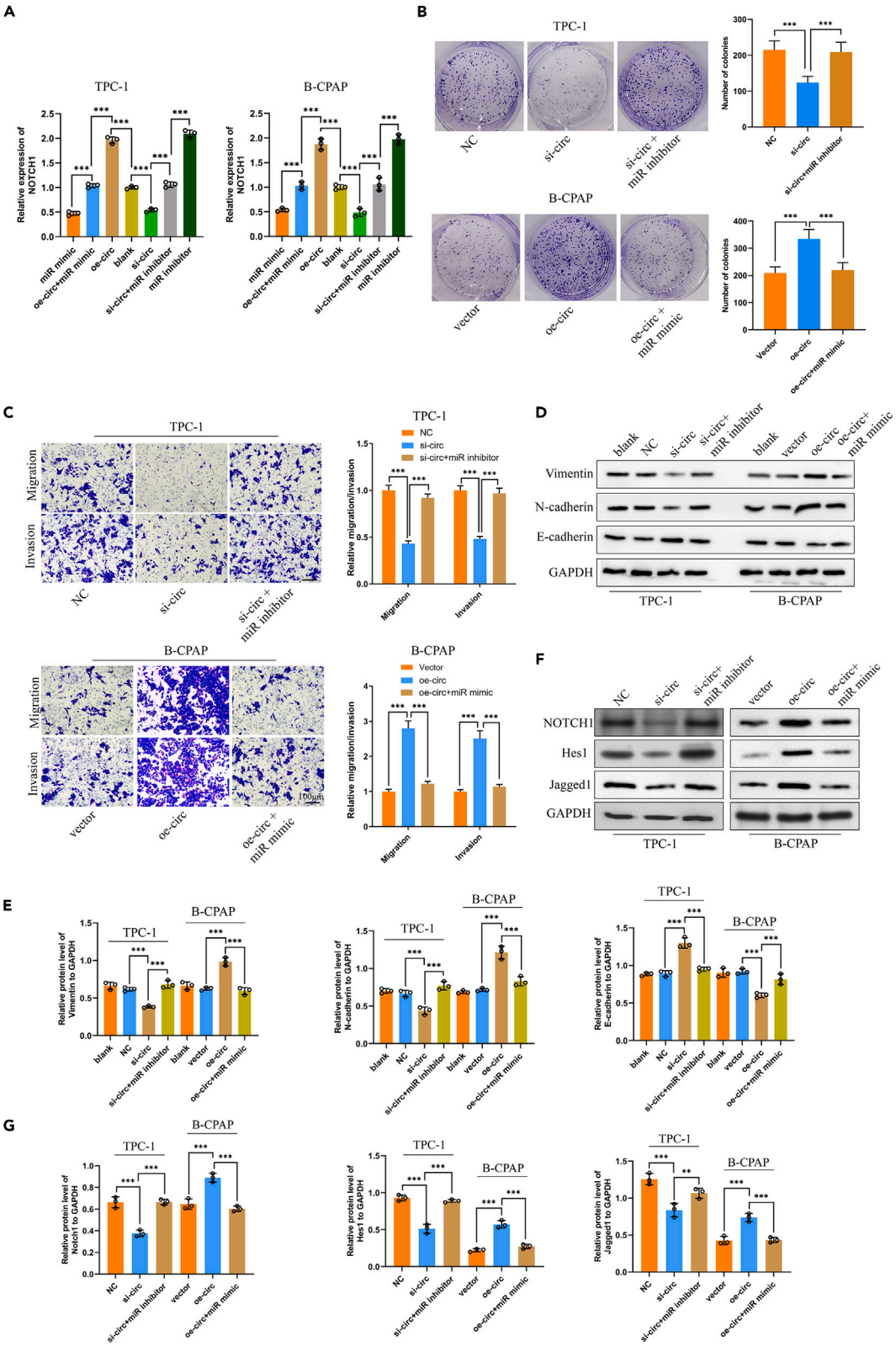
A
TPC-1
B-CPAP
Relative expression of NOTCH1
miR mimic
oe-circ+miR mimic
oe-circ
blank
si-circ
si-circ+miR inhibitor
miR inhibitor
B
TPC-1
NC
si-circ
si-circ + miR inhibitor
Number of colonies
B-CPAP
vector
oe-circ
oe-circ + miR mimic
C
TPC-1
Migration
Invasion
Relative migration/invasion
B-CPAP
100μm
D
blank
NC
si-circ
si-circ+ miR inhibitor
vector
oe-circ
oe-circ+ miR mimic
Vimentin
N-cadherin
E-cadherin
GAPDH
F
NOTCH1
Hes1
Jagged1
E
Relative protein level of Vimentin to GAPDH
Relative protein level of N-cadherin to GAPDH
Relative protein level of E-cadherin to GAPDH
G
Relative protein level of Notch1 to GAPDH
Relative protein level of Hes1 to GAPDH
Relative protein level of Jagged1 to GAPDH

Figure 7. "ceRNA" network verification and rescue experiments

(A–G) Relative NOTCH1 expression in TPC-1 and B-CPAP cell lines transfected with oe-circAGTPBP1, si-circAGTPBP1, or miR-34a-5p mimic, inhibitor, or control according to qRT-PCR analyses. Colony formation (B), Transwell assays (C), and assessment of EMT-associated proteins (D and E) and NOTCH signaling pathway proteins (F and G) by western blotting of TPC-1 and B-CPAP cells transfected with oe-circAGTPBP1, si-circAGTPBP1, or miR-34a-5p mimic, inhibitor, or control. Scale bar: 100 μm. Each experiment was repeated three times with triplicates. PTC, papillary thyroid cancer; qRT-PCR, quantitative real-time polymerase chain reaction; NC, normal control. Data are shown as the mean ± SD, **p < 0.01, ***p < 0.001 by one-way analysis of variance (ANOVA).

oncogenes in various cancers, including colon cancer, gastric cancer, and lung cancer.[21] However, little is known about the biological functions and mechanisms of circRNAs in PTC progression.

The present study investigated the potential role of circRNAs in PTC progression, which remains largely unknown. By analyzing the expression profile of circRNAs in PTC tissues and adjacent normal tissues, we found that circAGTPBP1 was upregulated in PTC tissues. *In vitro* and *in vivo* functional studies demonstrated that circAGTPBP1 could promote PTC migration, invasion, and EMT, suggesting its tumor-promoting role. Further investigations revealed that circAGTPBP1 could regulate the Notch signaling pathway via the miR-34a-5p/NOTCH1 axis as a "ceRNA" molecule. The results of this study provide some insights into the pathogenesis of PTC and reveal a potential therapeutic target for PTC treatment.

MiR-34a has been widely recognized as a significant tumor suppressor that plays crucial roles in various cancer-associated processes.[22] Many studies have reported that miR-34a is frequently downregulated in multiple cancers, leading to the loss of its tumor-suppressing effect.[23] In addition, miR-34a has been found to inhibit cancer cell migration and invasion by targeting the NOTCH1 signaling pathway,[24] which is consistent with our findings. A previous study by Liu et al.[25] reported that miR-34a was underexpressed in PTC and could modulate thyroid cancer cell proliferation and tumor growth. However, conflicting results have also been reported, suggesting that miR-34a may exert an oncogenic effect in PTC by targeting GAS1.[26] The inconsistent findings may be attributed to heterogeneity in patient characteristics, such as ethnic backgrounds and clinical and pathological stages, as well as differences in primer design.

NOTCH1 is a member of the Notch family, which has been implicated in various cancers, such as leukemia,[27] breast cancer,[28] and prostate cancer.[29] The role of NOTCH1 in tumorigenesis has been extensively studied in different types of cancers, including prostate cancer,[30] glioblastoma,[31] and head and neck squamous cell carcinoma.[32] NOTCH1 is closely associated with many signaling pathways involved in tumorigenesis, and its prognostic value has been well documented in recent years.[33] Moreover, NOTCH1 overexpression has been confirmed to be associated with resistance to cancer therapeutic strategies by many *in vitro* studies in many types of cancer.[34] Furthermore, many agents that inhibit NOTCH1 via numerous strategies have anticancer effects and promising therapeutic applications.[33] NOTCH1 has been extensively implicated in tumorigenesis and correlates with many signaling pathways that are involved in many types of cancers.[35] Additionally, NOTCH1 overexpression is associated with resistance to cancer therapeutic strategies, and agents that inhibit NOTCH1 have anticancer effects and promising therapeutic applications.[36] NOTCH1 has been widely reported as a target gene of miR-34a-5p in various types of tumors, including glioma,[37,38] and pancreatic cancer.[39] All these studies strongly support our result that NOTCH1 is a target gene of miR-34a-5p in PTC. In this study, the authors investigated the expression, biological function, and clinical implication of circAGTPBP1 in PTC via the miR-34a-5p/NOTCH1 axis.

Conclusion

In conclusion, this study highlights that a circRNA, circAGTPBP1, is significantly upregulated in PTC tissues and cells. The expression of circAGTPBP1 was found to be closely associated with tumor size, lymph node metastasis, and TNM stage. Functionally, circAGTPBP1 acts as an oncogene and promotes PTC migration, invasion, and metastasis both *in vitro* and *in vivo*. Mechanistically, circAGTPBP1 exerts its oncogenic activity by modulating the NOTCH signaling pathway via the miR-34a-5p/NOTCH1 axis. This study reveals the pathogenetic role of the circAGTPBP1/miR-34a-5p/NOTCH1 axis in PTC progression, and it provides insight into PTC carcinogenesis and aggressiveness. In addition, this study provides a potential screening method and therapeutic target for PTC, but further verification is required to determine if this axis applies to other types of thyroid cancer.

Limitations of the study

First, this study reveals one of the mechanisms of circAGTPBP1 in PTC from the perspective of ceRNA. It is unclear whether it also functions through other mechanisms, such as RBP interactions. Second, for a comprehensive understanding the function of circAGTPBP1 in PTC, it is necessary to consider the influence of the tumor microenvironment. Third, the sample size in our study was relatively small, which imposes limitations on our findings.

STAR★METHODS

Detailed methods are provided in the online version of this paper and include the following:

- KEY RESOURCES TABLE
- RESOURCE AVAILABILITY
  - Lead contact
  - Materials availability
  - Data and code availability
- EXPERIMENTAL MODEL AND STUDY PARTICIPANT DETAILS

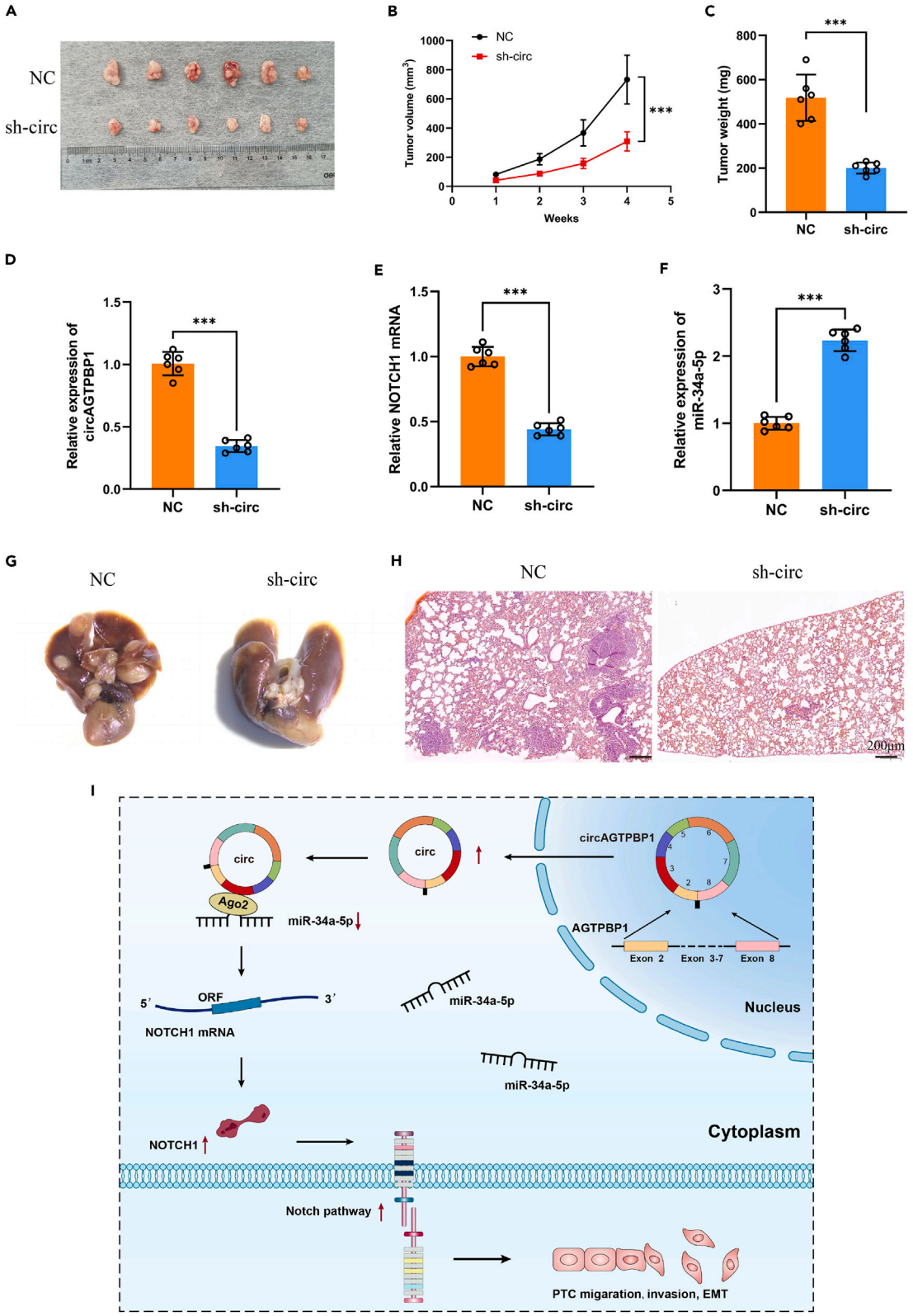
A
NC
sh-circ
B
NC
sh-circ
Tumor volume (mm3)
Weeks
***
C
Tumor weight (mg)
NC
sh-circ
***
D
Relative expression of circAGTPBP1
NC
sh-circ
***
E
Relative NOTCH1 mRNA
NC
sh-circ
***
F
Relative expression of miR-34a-5p
NC
sh-circ
***
G
NC
sh-circ
H
NC
sh-circ
200μm
I
circ
Ago2
miR-34a-5p
ORF
5′
3′
NOTCH1 mRNA
NOTCH1
Notch pathway
circ
circAGTPBP1
AGTPBP1
Exon 2
Exon 3-7
Exon 8
miR-34a-5p
miR-34a-5p
Nucleus
Cytoplasm
PTC migration, invasion, EMT

Figure 8. circAGTPBP1 knockdown inhibited PTC growth *in vivo*

(A–H) Subcutaneous tumor tissues in nude mice injected with TPC-1 cells transfected with si-circAGTPBP1 and NC. Tumor volume (B) and weight (C) in the si-circAGTPBP1 and NC groups. Relative expression of circAGTPBP1 (D), NOTCH1 (E), and miR-34a-5p (F) in tumor tissues in the si-circAGTPBP1 and NC groups by qRT-PCR. Representative images (G) and H&E staining analysis (H) of lungs dissected from mice with intravenous injection of NC or sh-circAGTPBP1. Scale bar: 200 μm. (I) Schematic diagram showing the mechanism by which circAGTPBP1 affects the progression of PTC. Each experiment was repeated three times with triplicates. PTC, papillary thyroid cancer; qRT-PCR, quantitative real-time polymerase chain reaction; NC, normal control. Data are shown as the mean ± SD, $^{**}p < 0.01$, $^{***}p < 0.001$ by Student's *t* test.

SUPPLEMENTAL INFORMATION

Supplemental information can be found online at https://doi.org/10.1016/j.isci.2023.107564.

ACKNOWLEDGMENTS

This study is Supported by Ningbo Natural Science Foundation (No. 2023J322; 2021J313); HwaMei Research Foundation of Ningbo No.2 Hospital (No. 2022HMK40); Young Technical Backbone Talent of Health in Ningbo; Zhu Xiushan Talent Award Fund of Ningbo NO.2 Hospital; The Project of NINGBO Leading Medical & Health Discipline (No. 2022-F18).

AUTHOR CONTRIBUTIONS

L.D., W.D.Z., and Y.C.W.: study design and data analysis.

K.J.Y., and Q.L.: patient recruitment, data collection, and writing up of the first draft of the paper.

L.D., and X.J.W.: scientific advice, supervision, and drafting of the manuscript.

DECLARATION OF INTERESTS

The authors declare no conflict of interest.

Received: January 7, 2023
Revised: May 23, 2023
Accepted: August 2, 2023
Published: August 9, 2023

REFERENCES

1. Vaccarella, S., Franceschi, S., Bray, F., Wild, C.P., Plummer, M., and Dal Maso, L. (2016). Worldwide Thyroid-Cancer Epidemic? The Increasing Impact of Overdiagnosis. N. Engl. J. Med. *375*, 614–617. https://doi.org/10.1056/NEJMp1604412.
2. Chen, W., Zheng, R., Baade, P.D., Zhang, S., Zeng, H., Bray, F., Jemal, A., Yu, X.Q., and He, J. (2016). Cancer statistics in China, 2015. CA A Cancer J. Clin. *66*, 115–132. https://doi.org/10.3322/caac.21338.
3. Abdullah, M.I., Junit, S.M., Ng, K.L., Jayapalan, J.J., Karikalan, B., and Hashim, O.H. (2019). Papillary Thyroid Cancer: Genetic Alterations

and Molecular Biomarker Investigations. Int. J. Med. Sci. *16*, 450–460. https://doi.org/10.7150/ijms.29935.

4. He, H., Liyanarachchi, S., Li, W., Comiskey, D.F., Jr., Yan, P., Bundschuh, R., Turkoglu, A.M., Brock, P., Ringel, M.D., and de la Chapelle, A. (2021). Transcriptome analysis discloses dysregulated genes in normal appearing tumor-adjacent thyroid tissues from patients with papillary thyroid carcinoma. Sci. Rep. *11*, 14126. https://doi.org/10.1038/s41598-021-93526-9.
5. Memczak, S., Jens, M., Elefsinioti, A., Torti, F., Krueger, J., Rybak, A., Maier, L., Mackowiak, S.D., Gregersen, L.H., Munschauer, M., et al. (2013). Circular RNAs are a large class of animal RNAs with regulatory potency. Nature *495*, 333–338. https://doi.org/10.1038/nature11928.
6. Zlotorynski, E. (2015). Non-coding RNA: Circular RNAs promote transcription. Nat. Rev. Mol. Cell Biol. *16*, 206. https://doi.org/10.1038/nrm3967.
7. Qu, S., Zhong, Y., Shang, R., Zhang, X., Song, W., Kjems, J., and Li, H. (2017). The emerging landscape of circular RNA in life processes. RNA Biol. *14*, 992–999. https://doi.org/10.1080/15476286.2016.1220473.
8. Rybak-Wolf, A., Stottmeister, C., Glažar, P., Jens, M., Pino, N., Giusti, S., Hanan, M., Behm, M., Bartok, O., Ashwal-Fluss, R., et al. (2015). Circular RNAs in the Mammalian Brain Are Highly Abundant, Conserved, and Dynamically Expressed. Mol. Cell *58*, 870–885. https://doi.org/10.1016/j.molcel.2015.03.027.
9. Kristensen, L.S., Jakobsen, T., Hager, H., and Kjems, J. (2022). The emerging roles of circRNAs in cancer and oncology. Nat. Rev. Clin. Oncol. *19*, 188–206. https://doi.org/10.1038/s41571-021-00585-y.
10. Liu, L., Yan, C., Tao, S., and Wang, H. (2020). Circ_0058124 Aggravates the Progression of Papillary Thyroid Carcinoma by Activating LMO4 Expression via Targeting miR-370-3p. Cancer Manag. Res. *12*, 9459–9470. https://doi.org/10.2147/CMAR.S271778.
11. Qu, S., Liu, Z., Yang, X., Zhou, J., Yu, H., Zhang, R., and Li, H. (2018). The emerging functions and roles of circular RNAs in cancer. Cancer Lett. *414*, 301–309. https://doi.org/10.1016/j.canlet.2017.11.022.
12. Bi, W., Huang, J., Nie, C., Liu, B., He, G., Han, J., Pang, R., Ding, Z., Xu, J., and Zhang, J. (2018). CircRNA circRNA_102171 promotes papillary thyroid cancer progression through modulating CTNNBIP1-dependent activation of β-catenin pathway. J. Exp. Clin. Cancer Res. *37*, 275. https://doi.org/10.1186/s13046-018-0936-7.
13. Yao, Y., Chen, X., Yang, H., Chen, W., Qian, Y., Yan, Z., Liao, T., Yao, W., Wu, W., Yu, T., et al. (2019). Hsa_circ_0058124 promotes papillary thyroid cancer tumorigenesis and invasiveness through the NOTCH3/GATAD2A axis. J. Exp. Clin. Cancer Res. *38*, 318. https://doi.org/10.1186/s13046-019-1321-x.
14. Zhang, D., Tao, L., Xu, N., Lu, X., Wang, J., He, G., Tang, Q., Huang, K., Shen, S., and Chu, J. (2022). CircRNA circTIAM1 promotes papillary thyroid cancer progression through the miR-646/HNRNPA1 signaling pathway. Cell Death Dis. *8*, 21. https://doi.org/10.1038/s41420-021-00798-1.
15. Mathews, D.H., Disney, M.D., Childs, J.L., Schroeder, S.J., Zuker, M., and Turner, D.H. (2004). Incorporating chemical modification constraints into a dynamic programming algorithm for prediction of RNA secondary structure. Proc. Natl. Acad. Sci. USA *101*, 7287–7292. https://doi.org/10.1073/pnas.0401799101.
16. Zhang, L., Lian, R., Zhao, J., Feng, X., Ye, R., Pan, L., Wu, J., Li, M., Huan, Y., and Cai, J. (2019). IGFBP7 inhibits cell proliferation by suppressing AKT activity and cell cycle progression in thyroid carcinoma. Cell Biosci. *9*, 44. https://doi.org/10.1186/s13578-019-0310-2.
17. Song, E., Jeon, M.J., Oh, H.S., Han, M., Lee, Y.M., Kim, T.Y., Chung, K.W., Kim, W.B., Shong, Y.K., Song, D.E., and Kim, W.G. (2018). Do aggressive variants of papillary thyroid carcinoma have worse clinical outcome than classic papillary thyroid carcinoma. Eur. J. Endocrinol. *179*, 135–142. https://doi.org/10.1530/EJE-17-0991.
18. Vuong, H.G., Long, N.P., Anh, N.H., Nghi, T.D., Hieu, M.V., Hung, L.P., Nakazawa, T., Katoh, R., and Kondo, T. (2018). Papillary thyroid carcinoma with tall cell features is as aggressive as tall cell variant: a meta-analysis. Endocr. Connect. *7*, R286–R293. https://doi.org/10.1530/EC-18-0333.
19. Goodall, G.J., and Wickramasinghe, V.O. (2021). RNA in cancer. Nat. Rev. Cancer *21*, 22–36. https://doi.org/10.1038/s41568-020-00306-0.
20. Lodde, V., Murgia, G., Simula, E.R., Steri, M., Floris, M., and Idda, M.L. (2020). Long Noncoding RNAs and Circular RNAs in Autoimmune Diseases. Biomolecules *10*, 1044. https://doi.org/10.3390/biom10071044.
21. Chen, L., and Shan, G. (2021). CircRNA in cancer: Fundamental mechanism and clinical potential. Cancer Lett. *505*, 49–57. https://doi.org/10.1016/j.canlet.2021.02.004.
22. Kalfert, D., Ludvikova, M., Pesta, M., Ludvik, J., Dostalova, L., and Kholová, I. (2020). Multifunctional Roles of miR-34a in Cancer: A Review with the Emphasis on Head and Neck Squamous Cell Carcinoma and Thyroid Cancer with Clinical Implications. Diagnostics *10*, 563. https://doi.org/10.3390/diagnostics10080563.
23. Nie, D., Fu, J., Chen, H., Cheng, J., and Fu, J. (2019). Roles of MicroRNA-34a in Epithelial to Mesenchymal Transition, Competing Endogenous RNA Sponging and Its Therapeutic Potential. Int. J. Mol. Sci. *20*, 861. https://doi.org/10.3390/ijms20040861.
24. Xie, Y., Ma, X., Chen, L., Li, H., Gu, L., Gao, Y., Zhang, Y., Li, X., Fan, Y., Chen, J., and Zhang, X. (2017). MicroRNAs with prognostic significance in bladder cancer: a systematic review and meta-analysis. Sci. Rep. *7*, 5619. https://doi.org/10.1038/s41598-017-05801-3.
25. Liu, H., Deng, H., Zhao, Y., Li, C., and Liang, Y. (2018). LncRNA XIST/miR-34a axis modulates the cell proliferation and tumor growth of thyroid cancer through MET-PI3K-AKT signaling. J. Exp. Clin. Cancer Res. *37*, 279. https://doi.org/10.1186/s13046-018-0950-9.
26. Ma, Y., Qin, H., and Cui, Y. (2013). MiR-34a targets GAS1 to promote cell proliferation and inhibit apoptosis in papillary thyroid carcinoma via PI3K/Akt/Bad pathway. Biochem. Biophys. Res. Commun. *441*, 958–963. https://doi.org/10.1016/j.bbrc.2013.11.010.
27. Sanchez-Martin, M., and Ferrando, A. (2017). The NOTCH1-MYC highway toward T-cell acute lymphoblastic leukemia. Blood *129*, 1124–1133. https://doi.org/10.1182/blood-2016-09-692582.
28. Jiang, H., Zhou, C., Zhang, Z., Wang, Q., Wei, H., Shi, W., Li, J., Wang, Z., Ou, Y., Wang, W., et al. (2020). Jagged1-Notch1-deployed tumor perivascular niche promotes breast cancer stem cell phenotype through Zeb1. Nat. Commun. *11*, 5129. https://doi.org/10.1038/s41467-020-18860-4.
29. Rice, M.A., Hsu, E.C., Aslan, M., Ghoochani, A., Su, A., and Stoyanova, T. (2019). Loss of Notch1 Activity Inhibits Prostate Cancer Growth and Metastasis and Sensitizes Prostate Cancer Cells to Antiandrogen Therapies. Mol. Cancer Therapeut. *18*, 1230–1242. https://doi.org/10.1158/1535-7163.MCT-18-0804.
30. Leong, K.G., and Gao, W.Q. (2008). The Notch pathway in prostate development and cancer. Differentiation *76*, 699–716. https://doi.org/10.1111/j.1432-0436.2008.00288.x.
31. Hai, L., Zhang, C., Li, T., Zhou, X., Liu, B., Li, S., Zhu, M., Lin, Y., Yu, S., Zhang, K., et al. (2018). Notch1 is a prognostic factor that is distinctly activated in the classical and proneural subtype of glioblastoma and that promotes glioma cell survival via the NF-κB(p65) pathway. Cell Death Dis. *9*, 158. https://doi.org/10.1038/s41419-017-0119-z.
32. Mao, L., Zhao, Z.L., Yu, G.T., Wu, L., Deng, W.W., Li, Y.C., Liu, J.F., Bu, L.L., Liu, B., Kulkarni, A.B., et al. (2018). γ-Secretase inhibitor reduces immunosuppressive cells and enhances tumour immunity in head and neck squamous cell carcinoma. Int. J. Cancer *142*, 999–1009. https://doi.org/10.1002/ijc.31115.
33. Gharaibeh, L., Elmadany, N., Alwosaibai, K., and Alshaer, W. (2020). Notch1 in Cancer Therapy: Possible Clinical Implications and Challenges. Mol. Pharmacol. *98*, 559–576. https://doi.org/10.1124/molpharm.120.000006.
34. Phillips, E., Lang, V., Bohlen, J., Bethke, F., Puccio, L., Tichy, D., Herold-Mende, C., Hielscher, T., Lichter, P., and Goidts, V. (2016). Targeting atypical protein kinase C iota reduces viability in glioblastoma stem-like cells via a notch signaling mechanism. Int. J. Cancer *139*, 1776–1787. https://doi.org/10.1002/ijc.30234.
35. Meurette, O., and Mehlen, P. (2018). Notch Signaling in the Tumor Microenvironment. Cancer Cell *34*, 536–548. https://doi.org/10.1016/j.ccell.2018.07.009.
36. Yamashita, A.S., Geraldo, M.V., Fuziwara, C.S., Kulcsar, M.A.V., Friguglietti, C.U.M., da Costa, R.B., Baia, G.S., and Kimura, E.T. (2013). Notch pathway is activated by MAPK signaling and influences papillary thyroid cancer proliferation. Transl. Oncol. *6*, 197–205. https://doi.org/10.1593/tlo.12442.
37. Li, Y., Guessous, F., Zhang, Y., Dipierro, C., Kefas, B., Johnson, E., Marcinkiewicz, L., Jiang, J., Yang, Y., Schmittgen, T.D., et al. (2009). MicroRNA-34a inhibits glioblastoma growth by targeting multiple oncogenes. Cancer Res. *69*, 7569–7576. https://doi.org/10.1158/0008-5472.CAN-09-0529.
38. Xu, H., Zhang, Y., Qi, L., Ding, L., Jiang, H., and Yu, H. (2018). NFIX Circular RNA Promotes Glioma Progression by Regulating miR-34a-5p via Notch Signaling Pathway. Front. Mol. Neurosci. *11*, 225. https://doi.org/10.3389/fnmol.2018.00225.
39. Gao, Y., Yang, M., Wei, L., Liang, X., Wu, F., Huang, Y., and Yang, T. (2020). miR-34a-5p Inhibits Cell Proliferation, Migration and Invasion Through Targeting JAG1/Notch1 Pathway in HPV-Infected Human Epidermal Keratinocytes. Pathol. Oncol. Res. *26*,

1851–1859. https://doi.org/10.1007/s12253-019-00782-2.

40. Liu, M., Wang, Q., Shen, J., Yang, B.B., and Ding, X. (2019). Circbank: a comprehensive database for circRNA with standard nomenclature. RNA Biol. *16*, 899–905. https://doi.org/10.1080/15476286.2019.1600395.

41. Li, J.H., Liu, S., Zhou, H., Qu, L.H., and Yang, J.H. (2014). starBase v2.0: decoding miRNA-ceRNA, miRNA-ncRNA and protein-RNA interaction networks from large-scale CLIP-Seq data. Nucleic Acids Res. *42*, D92–D97. https://doi.org/10.1093/nar/gkt1248.

42. Paraskevopoulou, M.D., Georgakilas, G., Kostoulas, N., Vlachos, I.S., Vergoulis, T., Reczko, M., Filippidis, C., Dalamagas, T., and Hatzigeorgiou, A.G. (2013). DIANA-microT web server v5.0: service integration into miRNA functional analysis workflows. Nucleic Acids Res. *41*, W169–W173. https://doi.org/10.1093/nar/gkt393.

43. Tokar, T., Pastrello, C., Rossos, A.E.M., Abovsky, M., Hauschild, A.C., Tsay, M., Lu, R., and Jurisica, I. (2018). mirDIP 4.1-integrative database of human microRNA target predictions. Nucleic Acids Res. *46*, D360–D370. https://doi.org/10.1093/nar/gkx1144.

44. Karagkouni, D., Paraskevopoulou, M.D., Chatzopoulos, S., Vlachos, I.S., Tastsoglou, S., Kanellos, I., Papadimitriou, D., Kavakiotis, I., Maniou, S., Skoufos, G., et al. (2018). DIANA-TarBase v8: a decade-long collection of experimentally supported miRNA-gene interactions. Nucleic Acids Res. *46*, D239–D245. https://doi.org/10.1093/nar/gkx1141.

STAR★METHODS

KEY RESOURCES TABLE

REAGENT or RESOURCE	SOURCE	IDENTIFIER
Antibodies		
Rabbit Polyclonal Anti-GZMB	Abcam	RRID: AB_881725
Rabbit Polyclonal Anti-vimentin	Abcam	RRID: AB_10562134
Rabbit Polyclonal Anti-N-cadherin	Proteintech Group	RRID: AB_2881610
Rabbit Polyclonal anti-E-cadherin	Proteintech Group	RRID: AB_10697811
Deposited data		
circRNA RNA-seq data	This paper	GEO:GSE237841
Experimental models: Cell lines		
TPC-1	Procell Life Science&Technology	Cat # CL-0643
B-CPAP	Chinese Academy of Sciences	Cat # SCSP-543
Experimental models: Organisms/strains		
BALB/c nude mice	Vital River Laboratories	N/A
Oligonucleotides		
circAGTPBP1 Forward: CTCTGTGAATTCAGTATCCTTAG	GenePharma	N/A
circAGTPBP1 Reverse: TGCAGATAATTTTATAAGACTGG	GenePharma	N/A
miR-34a-5p Forward: CGCGTGGCAGTGTCTTAGC	GenePharma	N/A
miR-34a-5p Reverse: GTCGTATCCAGTGCAGGGTC	GenePharma	N/A
miR-34a-5p RT Primer: GTCGTATCCAGTGCAGGGTCCGAGGTATTCGCACTGGATACGACACAACC	GenePharma	N/A
Si-circAGTPBP1-1 Target: AAGAATTCCAGTCTTATAAAATT	GenePharma	N/A
Forward: UUUUAUAAGACUGGAAUUCUU	GenePharma	N/A
Reverse: GAAUUCCAGUCUUAUAAAAUU	GenePharma	N/A
Si-circAGTPBP1-2 Target: TCCAGTCTTATAAAATTATCTGC	GenePharma	N/A
Forward: AGAUAAUUUUAUAAGACUGGA	GenePharma	N/A
Reverse: CAGUCUUAUAAAAUUAUCUGC	GenePharma	N/A
Si-circAGTPBP1-3 Target: GAGGACTTAATGGTACAGATTCA	GenePharma	N/A
Forward:AAUCUGUACCAUUAAGUCCUC	GenePharma	N/A
Reverse: GGACUUAAUGGUACAGAUUCA	GenePharma	N/A
Sh-circAGTPBP1 Target: CGGGTCTCATGAAATTATCTG	GenePharma	N/A
Forward: CCGGCGGGTCTCATGAAATTATCTGCTCGAGCAGATAATTTCATGA GACCCGTTTTTG	GenePharma	N/A
Reverse: AATTCAAAAACGGGTCTCATGAAATTATCTGCTCGAGCAGATAATTT CATGAGACCCG	GenePharma	N/A
Software and algorithms		
GraphPad Prism 9.0	GraphPad	N/A
ImageJ	NIH	N/A
SPSS 22.0	IBM	N/A

RESOURCE AVAILABILITY

Lead contact

Further information and requests for resources and reagents should be directed to and will be fulfilled by the lead contact, Xianjiang Wu (wuxianjiangtg@163.com).

Materials availability

The study did not generate new unique reagents.

Data and code availability

The circRNA RNA-seq data in this study have been deposited in the GEO database with the accession codes GSE237841, which is publicly available.
This paper does not report original code.
Any additional information is available from the lead contact upon request.

EXPERIMENTAL MODEL AND STUDY PARTICIPANT DETAILS

Patient samples

This study was approved by the ethics committee of our hospital in accordance with the Declaration of Helsinki (approval No. YJ-NBEY-KY-2021-182-01). PTC and paired adjacent normal tissues (3 cm away from the tumor edge) were obtained from 54 patients (Ningbo No.2 Hospital, East Asian population, mean age: 44.5 y, including 17 males and 37 females) with a confirmed pathological PTC diagnosis during surgery by two specialized pathologists. Written informed consent was obtained from each enrolled patient. The collected samples were put into liquid nitrogen and stored at -80°C. A total of 8 samples, consisting of four PTC samples and four matching adjacent normal tissues, were selected for circRNA sequencing and bioinformatic analysis.

Cell culture and treatment

The human normal thyroid follicular epithelial cell line (Nthy-ori 3-1) and PTC cell lines, including TPC-1, B-CPAP, KTC-1, K1, and IHH-4, were used for further experiments. The Nthy-ori 3-1 cells and PTC cell lines were maintained in RPMI-1640 medium with 10% fetal bovine serum and 100 U/ml streptomycin and penicillin. MEM nonessential amino acid solution (NEAA 100X, Gibco, Grand Island, NY, USA) was added to the B-CPAP cell line. All the cell lines were maintained in humidified conditions at 37°C in 5% CO_2.

Xenografts in nude mice and lung metastasis model

All animal experiments were approved by the Ethics Committee of Hwa Mei Hospital, University of Chinese Academy of Sciences (No. GK-2022-LW-0001) according to the guidelines of the Guide for the Care and Use of Laboratory Animals of the China National Institutes of Health. Female nude mice (female, 5 weeks old) were subcutaneously injected with 5×10^6 TPC-1 cells transfected with control or sh-circAGTPBP1 (n = 6 per group). The tumor length and width were measured by Vernier calipers (once a week for 5 weeks). The tumor volume was calculated as follows: volume (mm3) = (length × width^2)/2. Five weeks after injection, the mice were sacrificed, and the tumors were harvested and weighed. The *in vivo* tumor metastasis model was constructed through the administration of 5×10^6 TPC-1 cells transfected with control or sh-circAGTPBP1 (n = 6 per group) via the tail vein. The lungs were dissected from mice, photographed, and stained with matoxylin and eosin (H&E) .

METHOD DETAILS

CircRNA/mRNA sequencing and bioinformatic analysis

RNA extraction and circRNA/mRNA sequencing were conducted by OE Biotechnology Co., Ltd. (Shanghai, China). In brief, total RNA was extracted from the obtained tissue samples using the mirVana miRNA Isolation Kit (Ambion) according to the manufacturer's protocol. An Agilent 2100 Bioanalyzer (Agilent Technologies, Santa Clara, CA, USA) was used for RNA integrity evaluation. The samples with an RNA integrity number (RIN) $\geq$ 7 were subjected to subsequent analysis. TruSeq Stranded Total RNA with Ribo-Zero Gold was used to construct the libraries following the manufacturer's instructions. The libraries were then sequenced using the Illumina sequencing platform (HiSeqTM 2500), and 150 bp/125 bp paired-end reads were generated. Differential circRNA/mRNA screening was performed at a threshold of $|\log_2$-fold change (FC)| > 2 and P value < 0.05 using the negative binomial distribution test method (NB) by R software. The target miRNAs of candidate circRNAs were identified using the databases of circBank[40] and starBase.[41] The target mRNAs of candidate miRNAs were identified using the databases of starBase,[41] microT,[42] miRanda (miranda.org), miRmap (https://mirmap.ezlab.org/), PITA (https://omictools.com/pita-tool), PicTar (https://pictar.mdc-berlin.de/), TargetScan (http://www.targetscan.org/vert_80/), miRDIP,[43] Tarbase,[44] and Funrich software (http://www.funrich.org/) tools.

RNA extraction and quantitative real-time polymerase chain reaction (qRT-PCR)

Total RNA was extracted with TRIzol reagent (Invitrogen, Carlsbad, CA, USA) following the manufacturer's instructions. The quantity and quality of RNA were determined with a Nanodrop and a bioanalyzer (Agilent Inc., Waldbronn, Germany). The qRT–PCR assay was performed using SYBR Green PCR master mix (Qiagen). circRNA/miRNA or mRNA expression was normalized to U6 or GAPDH to obtain relative expression values based on the $2^{-\Delta\Delta Ct}$ method. All assays were performed with triplicates and repeated three times. Primer sequences are presented in table.

Nucleic acid electrophoresis

Nucleic acid electrophoresis was performed as described below. Two percent agarose gel electrophoresis was used to separate the cDNA and gDNA PCR products with TAE buffer. Electrophoresis was performed at 100 V for 30 min to separate the DNA. Marker L (50-500 bp) (Sango Biotech, China) was used as the DNA marker, and the bands were visualized by UV irradiation.

RNase R treatment

RNase R treatment was performed as described below. In brief, 2 μg of total RNA was incubated at 37°C for 15 min with or without RNase R (3 U/μg, Geneseed, Guangzhou, China). RNA samples were then reverse transcribed using divergent and convergent primers. Next, qRT–PCR was performed for the quantification of circRNA.

RNA immunoprecipitation (RIP) assay

As described below, the Ago-RIP assay was performed using the Magna RIP RNA-Binding Protein IP Kit (Millipore, Billerica, MA, USA). TPC-1 and B-CPAP cells stably transfected with the miR-34a-5p mimic or control were lysed with anti-Argonaute 2 (Ago2) or control rabbit IgG (Abcam, MA, USA)-conjugated beads. Total RNA was isolated for further qRT–PCR analyses of circRNA and miRNA.

Fluorescence *in situ* hybridization (FISH)

FISH analyses were conducted in thyroid gland tissues and cells according to the manufacturer's instructions. In brief, frozen tissues or cells were fixed with 4% paraformaldehyde (Servicebio, Shanghai, China), incubated with Proteinase K working solution (Servicebio), and prehybridized with a prehybridization solution. Sections were then hybridized with a FAM-conjugated circAGTPBP1 probe or CY3-conjugated miR-34a-5p probe overnight and counterstained with DAPI. Finally, sections were observed and photographed using a NIKON biological microscope (Nikon, Tokyo, Japan). The sequences used for FISH probes are shown in table.

Primers sequences

Name	Sequence (5′–3′)
qRT-PCR	
circAGTPBP1	
Forward	CTCTGTGAATTCAGTATCCTTAG
Reverse	TGCAGATAATTTTATAAGACTGG
miR-34a-5p	
Forward	CGCGTGGCAGTGTCTTAGC
Reverse	GTCGTATCCAGTGCAGGGTC
RT Primer	GTCGTATCCAGTGCAGGGTCCGAG GTATTCGCACTGGATACGACACAACC
miR-145-5p	
Forward	CTCGGTCCAGTTTTCCCAGG
Reverse	GTCGTATCCAGTGCAGGGTC
RT Primer	GTCGTATCCAGTGCAGGGTCCGAGGT ATTCGCACTGGATACGACAGGGAT
NOTCH1	
Forward	CGTCAACGCCGTAGATGACC
Reverse	CCGTTCTTCAGGAGCACAACT
AGTPBP1	

(*Continued on next page*)

Continued

Name	Sequence (5′–3′)
Forward	ATGAATGCCAGCAAAGAATCTCC
Reverse	CAGAGCCCCATTAATTCTAGCC
GAPDH	
Forward	TCCTGGGCTACACTGAGCAC
Reverse	CTGTTGCTGTAGCCAAATTCGTTG
U6	
Forward	ATTGGAACGATACAGAGAAGATT
Reverse	GGAACGCTTCACGAATTTG
miR-34a-5p mimic	
Sense	UGGCAGUGUCUUAGCUGGUUGU
Antisense	ACAACCAGCUAAGACACUGCCA
Mimic control	
Sense	ACCUGCACUCCCUUGGAUUGU
Antisense	ACAAUCCAAGGGAGUGCAGGU
miR-34a-5p inhibitor	
Sense	ACAACCAGCUAAGACACUGCCA
Inhibitor control	
Sense	ACAAUCCAAGGGAGUGCAGGU
Si-circAGTPBP1-1	Target: AAGAATTCCAGTCTTATAAAATT
Forward	UUUUAUAAGACUGGAAUUCUU
Reverse	GAAUUCCAGUCUUAUAAAAUU
Si-circAGTPBP1-2	Target: TCCAGTCTTATAAAATTATCTGC
Forward	AGAUAAUUUUAUAAGACUGGA
Reverse	CAGUCUUAUAAAAUUAUCUGC
Si-circAGTPBP1-3	Target: GAGGACTTAATGGTACAGATTCA
Forward	AAUCUGUACCAUUAAGUCCUC
Reverse	GGACUUAAUGGUACAGAUUCA
Si-circAGTPBP1-control	Target:ATACAGGCGGCTGTGCGCGGCAC
Forward	GCCGCGCACAGCCGCCUGUAU
Reverse	ACAGGCGGCUGUGCGCGGCAC
Sh-circAGTPBP1	Target:CGGGTCTCATGAAATTATCTG
Forward	CCGGCGGGTCTCATGAAATTATCTGCTCGA GCAGATAATTTCATGAGACCCGTTTTTG
Reverse	AATTCAAAAACGGGTCTCATGAAATTATCTG CTCGAGCAGATAATTTCATGAGACCCG
FISH	
Cy3-circAGTPBP1	ATAATTGCAGATAATTTTATAAGACTGGAATT
FAM-miR-34a-5p	ACAACCAGCTAAGACACTGCCA

qRT-PCR, quantitative real time-polymerase chain reaction; FISH, fluorescence *in situ* hybridization.

Cell transfection

CircAGTPBP1 siRNA, overexpression vectors, and the miR-34a-5p mimic and inhibitor were purchased from GenePharma (Shanghai, China). The sequence of circAGTPBP1 was inserted into pcDNA3.1 (GenePharma) at the BamHI site for the construction of circAGTPBP1 overexpression. Three circAGTPBP1 siRNAs were designed, synthesized, and transfected into TPC-1 and B-CPAP cells using Lipofectamine 3000 (Invitrogen) following the manufacturer's instructions. After transfection for 48 h, qRT–PCR was performed to assess the transfection efficiency.

Dual-luciferase reporter assay

The sequences of circAGTPBP1 and the NOTCH1 mRNA 3'UTR were amplified by PCR and cloned into the pmirGLO dual-luciferase vector. TPC-1 and B-CPAP cells were transfected with the corresponding vectors (approximately 50 ng) together with the miR-34a-5p mimic or mimic control (approximately 25 ng) using Lipofectamine 3000 reagent (Invitrogen). After 2 days, the luciferase activity was detected using the dual-luciferase reporter assay system (Hanbio, Shanghai, China), and firefly luciferase activity relative to Renilla luciferase activity was calculated.

Western blotting

Proteins in PTC cells were extracted using RIPA lysis buffer (cat. #P0013, Beyotime, Shanghai, China) and quantified with a bicinchoninic acid (BCA) kit (cat. #P0009, Beyotime, China). Equal amounts of protein lysates were extracted by 10% SDS–PAGE and electroblotted onto polyvinylidene fluoride (PVDF) membranes (Millipore, MA, USA). Membranes were blocked with 5% skim milk powder and incubated with primary antibodies anti-vimentin (cat. #ab92547, Abcam, Cambridge, UK), anti-N-cadherin (cat. #66219-1-Ig, Proteintech Group, Inc., Wuhan, China), anti-E-cadherin (cat. #20874-1-AP, Proteintech Group), anti-NOTCH1 (cat. #ab52627, Abcam), anti-Hes1 (cat. #ab71559, Abcam), anti-Jagged1 (cat. #ab300561, Abcam), and anti-GAPDH (cat. #ab8245, Abcam) overnight at 4°C. Then, the membranes were incubated with secondary antibody (Abcam) for 2 h. Finally, the blots were visualized by ECL reagent (Millipore, Germany) and analyzed by Image Lab Software.

Cell immunofluorescence (IF) staining

TPC-1 and B-CPAP cells were fixed in 4% paraformaldehyde and permeabilized by treatment with PBS containing 0.5% Triton X-100. Cells were blocked using 3% bovine serum albumin (BSA) containing 5% fetal bovine serum (FBS) and 0.025% Triton X-100 at room temperature. Cells were further incubated with primary anti-N-cadherin (cat. #66219-1-Ig, Proteintech Group) and anti-E-cadherin (cat. #20874-1-AP, Proteintech Group) at 4°C overnight. Cells were then washed and incubated with appropriate secondary antibodies. Afterward, the nuclei were counterstained with DAPI for 5 min. Finally, the cells were observed and imaged using a confocal microscope (NIKON ECLIPSE C1).

Biotin-coupled probe RNA pull down assay

Biotinylated circAGTPBP1 and miR-34a-5p pull-down assays were performed as described below. In brief, TPC-1 or B-CPAP cells (1×10^7) were harvested, lysed, and sonicated. The probe was then incubated with probes-M280 streptavidin Dynabeads (Invitrogen) at 25°C for 2 h. Afterward, cell lysates were incubated with the probe-coated beads overnight at 4°C. After washing, the bead-bound RNA complexes were eluted and purified with TRIzol Reagent (Takara, Japan) for further qRT–PCR analyses.

Cell Counting kit-8 (CCK-8) assay

The proliferation ability of transfected cells was measured using a CCK-8 kit (cat: #CK04, Dojindo, Japan) based on the manufacturer's instructions. TPC-1 and B-CPAP cells were plated in a 96-well plate. Then, at 24, 48, and 72 h, CCK-8 reagent (10 μL, Dojindo, Japan) was added to the culture medium. After incubation at 37°C for 2 h, the optional density (OD) was detected at 450 nm with a microplate reader (BioTek Instruments, USA). Each experiment was repeated three times with triplicates.

Colony formation assay

Colony formation assays were performed according to the steps described below. In brief, TPC-1 and B-CPAP cells stably transfected with si-circAGTPBP1 or control were seeded in 12-well plates and cultured at 37°C for 8 days. After washing, the cells were fixed with 4% paraformaldehyde for 15 min and stained with 0.1% crystal violet. The number of colonies formed was analyzed under a microscope. Each experiment was repeated three times with triplicates.

5- Ethynyl-20-deoxyuridine (EdU) incorporation assay

Cell proliferation was assessed by EdU assay using an EdU detection kit (Ribobio, China) following the manufacturer's instructions. In brief, TPC-1 and B-CPAP cells were cultured for 24 h in 24-well plates. After incubation with 50 mM EdU solution for 2 h, the cells were fixed with 4% paraformaldehyde and permeabilized with 0.5% Triton X-100 for 5 min. After washing, the cells were stained using Apollo staining solution and Hoechst 33342 dye (Invitrogen, USA). The cells were observed and photographed under a fluorescence microscope (Olympus, Tokyo, Japan).

Wound healing assays

A wound healing assay was performed to assess the migration rate *in vitro*. TPC-1 and B-CPAP cells (5×10^5 cells) were cultured in six-well plates. After achieving 90% cell confluence, the medium was replaced with serum-free medium and incubated for 12 h. Afterward, 200 ml pipette tips were used to scratch the cells. Representative images were obtained under an inverted microscope (Nikon, Japan) at 0 h and after 24 h of incubation. The relative migration was calculated by the diminishing distance across the induced injury area normalized to the 0 h control.

Transwell migration and invasion assays

Transwell migration and invasion assays were performed using Transwell plates (Millipore) according to the manufacturer's protocol. In brief, TPC-1 and B-CPAP cells were seeded in the upper chambers with serum-free medium (200 μl). Transwell assays were performed using a Transwell chamber (Corning, NY, USA) covered with Matrigel mix (BD Biosciences, San Jose, CA, USA) for the invasion assay and without Matrigel mix for the migration assays. The bottom chamber was filled with DMEM with 10% FBS as a chemoattractant. After 24 h of incubation, the cells were fixed with 4% paraformaldehyde and stained with 0.1% crystal violet. The cells were photographed under an inverted light microscope (Zeiss, Primovert) and counted in five different fields.

QUANTIFICATION AND STATISTICAL ANALYSIS

Statistical analysis was performed using SPSS 22.0 (SPSS, Chicago, IL, USA) and GraphPad Prism 9.0 (GraphPad, San Diego, CA, USA) software. Student's t test, chi-square test, or one-way analysis of variance (ANOVA) was used for data analysis. A two-tailed $P < 0.05$ was considered to indicate statistical significance.